J|A|C|S ARTICLES

Published on Web 06/10/2010

Spectroscopic Comparison of Photogenerated Tryptophan Radicals in Azurin: Effects of Local Environment and Structure

Hannah S. Shafaat, Brian S. Leigh, Michael J. Tauber, and Judy E. Kim*

Department of Chemistry and Biochemistry, University of California at San Diego, La Jolla, California 92093

Received February 21, 2010; E-mail: judyk@ucsd.edu

Abstract: Tryptophan radicals play a significant role in mediating biological electron transfer. We report the photogeneration of a long-lived, neutral tryptophan radical (Az48W•) from the native residue tryptophan-48 in the hydrophobic core of azurin. The optical absorption, electron paramagnetic resonance, and resonance Raman spectra strongly support the formation of a neutral radical, and the data are consistent with direct electron transfer between tryptophan and the copper(II) center. Spectra of the long-lived Az48W• species are compared to those of a previously studied, solvent-exposed radical at position 108 to identify signatures of tryptophan radicals that are sensitive to the local environment. The absorption maxima of Az48W• display an ~23 nm hypsochromic shift in the nonpolar environment. The majority of the resonance Raman frequencies are downshifted by ~7 cm^{-1} relative to the solvent-exposed radical, and large changes in intensity are observed for some modes. The resonance Raman excitation profiles for Az48W• exhibit distinct maxima within the absorption envelope. Electron paramagnetic resonance spectroscopy yields spectra with partially resolved lines caused by hyperfine couplings; the differences between the coupling constants for the buried and solvent-exposed radical are primarily caused by variations in structure. The insights gained by electronic, vibrational, and magnetic resonance spectroscopy enhance our fundamental understanding of the effects of protein environment on radical properties. Hypotheses for the proton transfer pathway within azurin and a deprotonation rate of ~5×10^6 s^{-1} are proposed.

Introduction

Redox-active aromatic amino acids play critical roles as intermediates in a variety of biological electron transfer (ET) processes, including enzymatic and multistep electron transfer reactions.[1−8] The tyrosine radical was the first amino acid radical identified and has been well characterized.[9,10] Considerably fewer reports have focused on the tryptophan radical, which is also prevalent in proteins.[1,2,4,7] The oxidation reaction of tryptophan is complex because it is often accompanied by the loss of a proton under physiological conditions.[11,12] This propensity for proton loss indicates that tryptophan may participate in proton-coupled electron transfer (PCET) reactions, which are critical in numerous catalytic and energy conversion reactions.[13−15] Currently, a library of spectral properties and correlations with a tryptophan radical environment is not available, in contrast to the well-studied closed-shell tryptophan residue.[16−18] The missing depth of knowledge on tryptophan radical spectroscopy is one factor that has obstructed our understanding of tryptophan-mediated ET reactions. We have embarked on a comprehensive analysis of the radical in a protein environment to establish correlations between the spectral properties of tryptophan radicals and structure, solvent polarity, and hydrogen bonding.[19] These spectroscopic markers in turn may be utilized to provide insight into electron transfer kinetics and mechanisms.

Our initial aim has been characterization of amino acid radicals in the well-studied blue-copper ET protein azurin.

(1) Stubbe, J.; van der Donk, W. A. *Chem. Rev.* **1998**, *98*, 705–762.
(2) Aubert, C.; Vos, M. H.; Mathis, P.; Eker, A. P. M.; Brettel, K. *Nature* **2000**, *405*, 586–590.
(3) Pogni, R.; Baratto, M. C.; Giansanti, S.; Teutloff, C.; Verdin, J.; Valderrama, B.; Lendzian, F.; Lubitz, W.; Vazquez-Duhalt, R.; Basosi, R. *Biochemistry* **2005**, *44*, 4267–4274.
(4) Wiertz, F. G. M.; Richter, O. M. H.; Ludwig, B.; de Vries, S. *J. Biol. Chem.* **2007**, *282*, 31580–31591.
(5) Shih, C.; Museth, A. K.; Abrahamsson, M.; Blanco-Rodriguez, A. M.; Di Bilio, A. J.; Sudhamsu, J.; Crane, B. R.; Ronayne, K. L.; Towrie, M.; Vlček, A., Jr.; Richards, J. H.; Winkler, J. R.; Gray, H. B. *Science* **2008**, *320*, 1760–1762.
(6) Krauss, M.; Garmer, D. R. *J. Phys. Chem.* **1993**, *97*, 831–836.
(7) Huyett, J. E.; Doan, P. E.; Gurbiel, R.; Houseman, A. L. P.; Sivaraja, M.; Goodin, D. B.; Hoffman, B. M. *J. Am. Chem. Soc.* **1995**, *117*, 9033–9041.
(8) Sivaraja, M.; Goodin, D. B.; Smith, M.; Hoffman, B. M. *Science* **1989**, *245*, 738–740.
(9) Sjöberg, B. M.; Reichard, P.; Gräslund, A.; Ehrenberg, A. *J. Biol. Chem.* **1978**, *253*, 6863–6865.
(10) Hoganson, C. W.; Tommos, C. *Biochim. Biophys. Acta* **2004**, *1655*, 116–122.
(11) Solar, S.; Getoff, N.; Surdhar, P. S.; Armstrong, D. A.; Singh, A. *J. Phys. Chem.* **1991**, *95*, 3639–3643.
(12) DeFelippis, M. R.; Murthy, C. P.; Faraggi, M.; Klapper, M. H. *Biochemistry* **1989**, *28*, 4847–4853.
(13) Reece, S. Y.; Hodgkiss, J. M.; Stubbe, J.; Nocera, D. G. *Philos. Trans. R. Soc. London, Ser. B* **2006**, *361*, 1351–1364.
(14) Stubbe, J.; Nocera, D. G.; Yee, C. S.; Chang, M. C. Y. *Chem. Rev.* **2003**, *103*, 2167–2201.
(15) Sjodin, M.; Styring, S.; Wolpher, H.; Xu, Y. H.; Sun, L. C.; Hammarstrom, L. *J. Am. Chem. Soc.* **2005**, *127*, 3855–3863.
(16) Vivian, J. T.; Callis, P. R. *Biophys. J.* **2001**, *80*, 2093–2109.
(17) Auer, H. E. *J. Am. Chem. Soc.* **1973**, *95*, 3003–3011.
(18) Miura, T.; Takeuchi, H.; Harada, I. *J. Raman Spectrosc.* **1989**, *20*, 667–671.
(19) Shafaat, H. S.; Leigh, B. S.; Tauber, M. J.; Kim, J. E. *J. Phys. Chem. B* **2009**, *113*, 382–388.

10.1021/ja101322g

Azurin contains a single native tryptophan residue, tryptophan-48, in a hydrophobic region of the β-barrel core 10 Å from the copper center.[20] This tryptophan residue has previously been examined in the context of intramolecular ET pathways through azurin[21] and displays unique spectroscopic features, including the smallest Stokes shift observed for the tryptophan fluorescence in any natural protein. Furthermore, the fluorescence intensity is highly quenched in the holoprotein relative to the apo- species.[22,23] It has been proposed for over two decades that this fluorescence quenching derives from excited-state electron transfer between tryptophan and the copper(II) center;[24,25] however, this process has not been experimentally confirmed until now.

In a protein environment, the mechanism of electron ejection from tryptophan is complex. Ultraviolet excitation of aqueous tryptophan model compounds has been shown to directly produce the tryptophan cation radical Trp^{+}• ($pK_a \approx 4$) or the neutral radical Trp• depending on pH.[26−29] In peptide and protein systems that are engineered to photoinitiate ribonucleotide reductase activity, photoionization of tryptophan is followed by electron transfer from tyrosine to the tryptophan radical.[30−32] In other systems, such as the photolyases and cryptochromes, electron transfer along tryptophan and tyrosine residues is initiated by photoexcitation of an FAD cofactor, followed by electron abstraction from the aromatic amino acid.[33,34] While photoionization of tryptophan to generate a solvated electron and highly oxidizing tryptophan radical has been utilized to initiate intraprotein ET,[32] to the best of our knowledge, there have been no prior reports of direct ET from excited-state tryptophan to a redox cofactor in a protein system.

Magnetic and optical spectroscopies are the primary techniques for characterization of amino acid radicals in natural protein systems. Much of the knowledge of amino acid radicals in proteins has been gained through electron paramagnetic resonance (EPR) and related electron magnetic-resonance techniques.[35,36] EPR spectra provide direct evidence of the spin density, electronic structure, and geometry of organic radical species.[37] High-frequency ($\geq$95 GHz) and multifrequency EPR studies are also able to provide valuable insights into the structure and immediate environment around the radical.[38−42] The information obtained through EPR spectroscopy is complementary to that obtained from optical and vibrational spectroscopy. However, despite some experimental advantages, absorption and resonance Raman (RR) spectroscopies have seen limited application in the study of tryptophan radicals within protein systems.[2,19,43] Collectively, these methods allow determination of the radical protonation state, conformation, environment hydrophobicity, and hydrogen bonding within a protein matrix. A systematic correlation between these three spectroscopic techniques will facilitate full characterization of both long-lived and transient neutral and cationic tryptophan radicals.

The goal of the current work is to utilize multiple spectroscopic tools to characterize a tryptophan radical in different protein environments. We have observed photoinduced reduction of the Cu(II) center from the native tryptophan-48 residue in a tyrosine-deficient mutant of azurin and report here on the electronic, magnetic, and vibrational spectra of the oxidized neutral tryptophan radical, Az48W•. The properties of this long-lived radical in its natural hydrophobic pocket are compared to those of a tryptophan radical in a partially solvent-exposed environment at position 108 generated in a rhenium-labeled azurin mutant (ReAz108W•).[19,44] This comparison enables identification of spectral signatures of tryptophan radicals that are sensitive to the local environment. Electron and proton transfer pathways and kinetics are discussed.

Materials and Methods

Materials were purchased from Fisher Scientific and used as received unless otherwise noted. D_2O (>99% isotopic purity) was obtained from Acros Organics.

Sample Preparation and Labeling. Expression, isolation, purification, labeling, metal exchange, and characterization of *Pseudomonas aeruginosa* azurin mutants with single tryptophan residues at positions 108 [W48F/Y72F/H83Q/Q107H/Y108W]-AzCu(II) (**Az108W**) and 48 [Y72F/Y108F]AzCu(II) (**Az48W**) were carried out as previously described.[44,45] Unlabeled protein samples were prepared by dilution of a >1 mM stock solution into an appropriate buffer immediately prior to the experiment. The rhenium-labeled Az108W mutant [Re(I)$(CO)_3$(4,7-dimethyl-1,10-phenanthroline)(H107)]Az(108W), **ReAz108W**, was prepared by

(20) Nar, H.; Messerschmidt, A.; Huber, R.; Vandekamp, M.; Canters, G. W. *J. Mol. Biol.* **1991**, *221*, 765–772.
(21) Farver, O.; Skov, L. K.; Young, S.; Bonander, N.; Karlsson, B. G.; Vanngard, T.; Pecht, I. *J. Am. Chem. Soc.* **1997**, *119*, 5453–5454.
(22) Kroes, S. J.; Canters, G. W.; Gilardi, G.; van Hoek, A.; Visser, A. *Biophys. J.* **1998**, *75*, 2441–2450.
(23) Gilardi, G.; Mei, G.; Rosato, N.; Canters, G. W.; Finazziagro, A. *Biochemistry* **1994**, *33*, 1425–1432.
(24) Petrich, J. W.; Longworth, J. W.; Fleming, G. R. *Biochemistry* **1987**, *26*, 2711–2722.
(25) Hansen, J. E.; Longworth, J. W.; Fleming, G. R. *Biochemistry* **1990**, *29*, 7329–7338.
(26) Stevenson, K. L.; Papadantonakis, G. A.; LeBreton, P. R. *J. Photochem. Photobiol., A* **2000**, *133*, 159–167.
(27) Gai, F.; Rich, R. L.; Petrich, J. W. *J. Am. Chem. Soc.* **1994**, *116*, 735–746.
(28) Peon, J.; Hess, G. C.; Pecourt, J. M. L.; Yuzawa, T.; Kohler, B. *J. Phys. Chem. A* **1999**, *103*, 2460–2466.
(29) Kandori, H.; Borkman, R. F.; Yoshihara, K. *J. Phys. Chem.* **1993**, *97*, 9664–9667.
(30) Sloper, R. W.; Land, E. J. *Photochem. Photobiol.* **1980**, *32*, 687–689.
(31) Reece, S. Y.; Stubbe, J.; Nocera, D. G. *Biochim. Biophys. Acta* **2005**, *1706*, 232–238.
(32) Chang, M. C. Y.; Yee, C. S.; Stubbe, J.; Nocera, D. G. *Proc. Natl. Acad. Sci. U.S.A.* **2004**, *101*, 6882–6887.
(33) Aubert, C.; Mathis, P.; Eker, A. P. M.; Brettel, K. *Proc. Natl. Acad. Sci. U.S.A.* **1999**, *96*, 5423–5427.
(34) Giovani, B.; Byrdin, M.; Ahmad, M.; Brettel, K. *Nat. Struct. Biol.* **2003**, *10*, 489–490.
(35) Lendzian, F.; Sahlin, M.; MacMillan, F.; Bittl, R.; Fiege, R.; Potsch, S.; Sjöberg, B. M.; Gräslund, A.; Lubitz, W.; Lassmann, G. *J. Am. Chem. Soc.* **1996**, *118*, 8111–8120.
(36) Tommos, C.; Tang, X. S.; Warncke, K.; Hoganson, C. W.; Styring, S.; McCracken, J.; Diner, B. A.; Babcock, G. T. *J. Am. Chem. Soc.* **1995**, *117*, 10325–10335.
(37) Gerson, F.; Huber, W. *Electron Spin Resonance Spectroscopy for Organic Radicals*; Wiley-VCH: 2001; Vol. 1.
(38) Bleifuss, G.; Kolberg, M.; Potsch, S.; Hofbauer, W.; Bittl, R.; Lubitz, W.; Gräslund, A.; Lassmann, G.; Lendzian, F. *Biochemistry* **2001**, *40*, 15362–15368.
(39) Pogni, R.; Teutloff, C.; Lendzian, F.; Basosi, R. *Appl. Magn. Reson.* **2007**, *31*, 509–526.
(40) Ivancich, A.; Mattioli, T. A.; Un, S. *J. Am. Chem. Soc.* **1999**, *121*, 5743–5753.
(41) Stoll, S.; Gunn, A.; Brynda, M.; Sughrue, W.; Kohler, A. C.; Ozarowski, A.; Fisher, A. J.; Lagarias, J. C.; Britt, R. D. *J. Am. Chem. Soc.* **2009**, *131*, 1986–1995.
(42) Mobius, K.; Savitsky, A. *High-Field EPR Spectroscopy on Protein and Their Model Systems*; The Royal Society of Chemistry: Cambridge, 2009.
(43) Gurudas, U.; Schelvis, J. P. M. *J. Am. Chem. Soc.* **2004**, *126*, 12788–12789.
(44) Miller, J. E.; Gradinaru, C.; Crane, B. R.; Di Bilio, A. J.; Wehbi, W. A.; Un, S.; Winkler, J. R.; Gray, H. B. *J. Am. Chem. Soc.* **2003**, *125*, 14220–14221.
(45) Di Bilio, A. J.; Crane, B. R.; Wehbi, W. A.; Kiser, C. N.; Abu-Omar, M. M.; Carlos, R. M.; Richards, J. H.; Winkler, J. R.; Gray, H. B. *J. Am. Chem. Soc.* **2001**, *123*, 3181–3182.

dilution of a stock solution of 250 μM ReAz108W into an appropriate buffer, and an aliquot of 50 mM exogenous quencher, $[Co^{III}(NH_3)_5Cl]Cl_2$, in deionized water was added to this solution to obtain a final concentration of 5 mM $[Co^{III}(NH_3)_5Cl]^{2+}$. The sample was placed in an atmosphere-controlled 3 mm i.d. EPR tube for visible RR and EPR experiments. An atmosphere-controlled 2 mm $\times$1 cm cuvette was used for absorption experiments. The samples were deoxygenated on a vacuum line with repeated pump/purge cycles. For ultraviolet resonance Raman (UVRR) experiments, the sample was flowed once through a 100 μm i.d. quartz capillary and then discarded. Final protein concentrations were $\sim$50 μM (absorption and UVRR), and $\sim$100 μM (visible RR and EPR) in $\sim$20 mM phosphate (pH 7.2 or pD 7.6) or acetate (pH 4.0) buffers.

For experiments utilizing N_2O as an electron scavenger, samples were degassed on a vacuum line and backfilled with gaseous N_2O. The evacuation/backfill procedure was repeated three times to ensure saturation of the solution with N_2O.

Photolysis of Azurin Mutants. Photolysis of ReAz108W with $[Co(NH_3)_5Cl]^{2+}$ quencher in deoxygenated solution was achieved with the 355 nm third harmonic output from a Q-switched 20 Hz Nd:YAG laser (Quantel Brilliant) as described previously.[19] Samples were photolyzed for 10 s with $\sim$500 μJ pulses in a defocused beam ($\sim$5 mm diameter) to create the radical species **ReAz108W•**. Photolysis of Az48W in a deoxygenated solution was achieved using 280 nm light. An optical parametric oscillator (Opotek) pumped with 355 nm light at 20 Hz produced 560 nm light, which was passed through a β-barium borate (BBO) crystal to produce the 280 nm beam. Samples were photolyzed for 60 s (unless otherwise noted) with $\sim$30 μJ pulses in a defocused beam to create the radical species **Az48W•**. Photolysis with 290 and 230 nm yielded identical spectra but with different yields.

Absorption Spectroscopy. Absorption spectra of ReAz108W• and Az48W• in atmosphere-controlled quartz cuvettes were obtained using a UV−vis−NIR spectrophotometer (Shimadzu UV-3600). The absorption spectrum of each radical was determined by calculating a difference spectrum of sample before and after photolysis. The $[Co(NH_3)_5Cl]^{2+}$ quencher consumed in the ReAz108W• system has a negligible absorption (extinction coefficient <50 M^{-1} cm^{-1}) in the spectral region where the radical absorbs; thus, effects of small changes in quencher concentration were neglected.[46] The spectral bandwidth was 1 nm.

EPR Spectroscopy. X-band EPR spectra were obtained using a Bruker ELEXSYS E500 spectrometer equipped with a Bruker ER4131VT variable temperature unit. Spectra were recorded at 125 K. Values of the g-factor were determined with an accuracy of $\pm$0.0001 by calibration with a standard of solid 2,2-diphenyl-1-picrylhydrazyl (DPPH), $g = 2.0036$ and a standard of phosphorus-doped silicon powder sample, $g = 1.99891$.[47] EPR spectra of ReAz108W and Az48W samples were acquired before and after photolysis. Each spectrum was acquired for $\sim$15 min using a modulation frequency of 100 kHz, modulation amplitude of 1.0 G, and microwave power of $\sim$6.4 μW which was well below saturation levels. Spectra of ReAz108W and Az48W acquired prior to photolysis allowed removal of the background Cu(II) signal. The EPR spectra of ReAz108W• and Az48W• were obtained from scaled subtraction of spectra (after photolysis) − (before photolysis, spline fitted). In a separate set of experiments, the microwave power saturation behavior was monitored to examine dipolar coupling.[48]

Simulations of the powder pattern EPR spectra were performed using the EasySpin program for $S = {}^1/_2$ systems with anisotropic g-factors and hyperfine coupling constants.[49] This software is based on the second-order perturbation solution of the standard spin Hamiltonian. The SIMPLEX method is used to minimize the standard deviation between experimental and fitted spectra. Simulations of the two radicals were performed by allowing the hyperfine coupling constants (hfcc's) to vary over a reasonable range to find the best fit to the experimental spectra. Gaussian line widths were constrained to 4 G in the simulations.

Resonance Raman (RR) Spectroscopy. A mixed-gas Kr−Ar laser (Coherent Innova 70C) provided excitation at 458 nm (1.2 mW), 488 nm (11 mW), 514.5 nm (13 mW), 530.9 nm (13 mW), and 568.2 nm (11 mW). The beam was focused into an atmosphere-controlled EPR tube containing a sample at room temperature. Scattered light was collected at 90° relative to the incident beam by an F/1.2 camera lens and imaged onto the spectrograph entrance slit opened to 100 μm. Rayleigh scattering was rejected by an appropriate long-pass edge filter for each wavelength. Raman scattered light was dispersed in an F/5, 0.32 m spectrograph (Horiba Jobin Yvon iHR 320) equipped with a 1200 gr/mm grating and detected by a thermoelectrically cooled CCD detector (Horiba Jobin Yvon Synapse). The bandpass and accuracy were 8 cm^{-1} and $\pm$1 cm^{-1}, respectively. Samples were characterized by absorption spectroscopy immediately prior to RR experiments to ensure that the radical was present. RR spectra were collected for approximately 3 h, with rephotolysis approximately every 30 min during this period. There was no indication of photodamage during the RR experiments. RR spectra of the sample prior to photolysis were subtracted from post-photolysis spectra to remove peaks from solvent or the Cu(II) center. A broad background caused by laser light scattering and/or fluorescence was removed by subtraction of an interpolated fit to the background.

Resonance Raman cross sections were determined using the ratio of peak intensities between Az48W• peaks and the bleach of the Cu(II)-S(Cys) band at 408 cm^{-1}. The absolute RR cross sections for this mode were previously reported.[50] The values used for 488, 514.5, 530.9, and 568.2 nm were 0.3, 0.9, 2.38, and 6.79 $\times$ 10^{-10} $Å^2$/molecule, respectively; the latter two cross sections are reported experimental values, while the former two values were taken from the fitted data presented in this prior report.[50] Depolarization ratios of 0.4 and 0.35−0.45 (data not shown) for the copper and radical peaks, respectively, were used to determine the absolute Raman cross sections.[50]

Instrumentation for UVRR spectroscopy has been described in detail elsewhere and is included in the Supporting Information.[51]

Calculations and Mode Assignments. Calculations were performed using the Gaussian 03W quantum chemistry program operating on a Windows platform.[52] The geometry and harmonic vibrational frequencies of 3-ethylindole were calculated using DFT with the hybrid B3LYP functional. Calculations for the 3-ethylindole neutral radical and 3-ethylindole cation radical were performed using spin-unrestricted DFT with the B3LYP functional. A 6-31G(d) basis set was selected for all calculations. Molecular orbitals were generated and viewed using GaussView.[52]

Mode assignments for previously unassigned peaks were made by comparing results from calculations of the closed-shell 3-ethylindole (3EI) to 3-ethylindole neutral radical (3EI•) with the aid of software to visualize atomic displacements[53] as described in detail previously;[19] a summary of these results is presented in the Supporting Information. Unless otherwise noted, nomenclature used here follows standard mode descriptions in the literature[54] and all radical mode assignments listed here are identical to those previously reported for ReAz108W•.[19]

(46) Jackson, W. G.; Begbie, C. M.; Randall, M. L. *Inorg. Chim. Acta* **1983**, *70*, 7.
(47) Stesmans, A.; Devos, G. *Phys. Rev. B* **1986**, *34*, 6499–6502.
(48) Hirsh, D. J.; Brudvig, G. W. *Nat. Protoc.* **2007**, *2*, 1770–1781.
(49) Stoll, S.; Schweiger, A. *J. Magn. Reson.* **2006**, *178*, 42–55.
(50) Webb, M. A.; Kwong, C. M.; Loppnow, G. R. *J. Phys. Chem. B* **1997**, *101*, 5062–5069.
(51) Sanchez, K. M.; Neary, T. J.; Kim, J. E. *J. Phys. Chem. B* **2008**, *112*, 9507–9511.
(52) Frisch, M. J. T. *GaussView*; Gaussian Inc.: Wallingford, CT, 2004.
(53) Grafton, A. K. *J. Comput. Chem.* **2007**, *28*, 1290–1305.
(54) Harada, I.; Takeuchi, H. In *Spectroscopy of Biological Systems*; Clark, R. J. H., Hester, R. E., Eds.; John Wiley and Sons Ltd: Chichester, U.K., 1986.

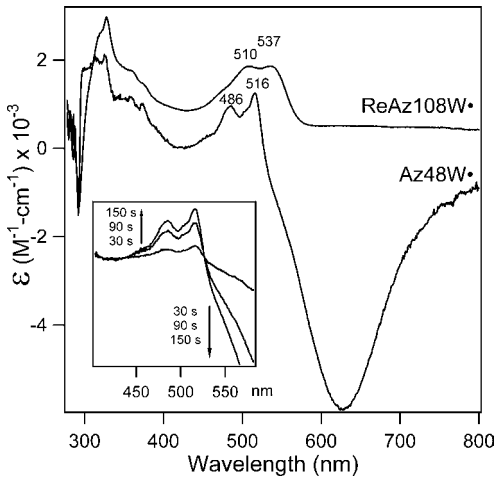

Figure 1. Difference absorption spectra of ReAz108W• and Az48W• in 20 mM phosphate buffer, pH 7.2. The spectrum of ReAz108W• is offset by 500 M^{-1} cm^{-1} for clarity. *Inset*: Difference absorption spectra of Az48W• with increasing photolysis time.

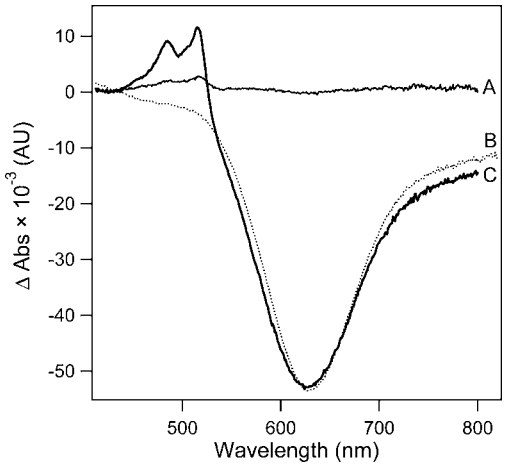

Figure 2. Difference absorption spectra after 280 nm photolysis of (A) Zn(II)Az48W, (B) Cu(II)Az48W + N_2O (saturated), and (C) Cu(II)Az48W in 20 mM phosphate buffer, pH 7.2. Absorbance for (B) has been scaled by a factor of 0.8.

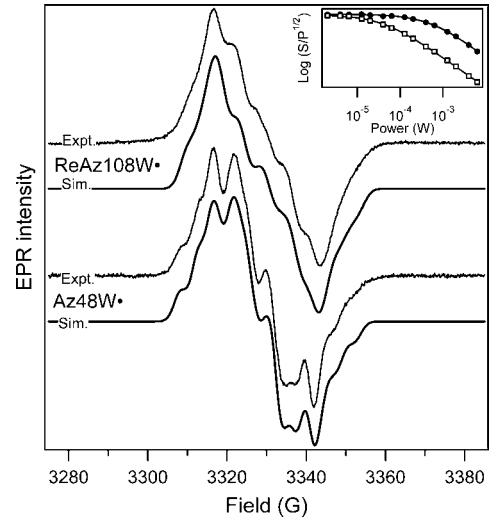

Figure 3. X-band (9.4 GHz) first-derivative EPR difference spectra ("Expt.") and simulations ("Sim.") at 125 K of ReAz108W• and Az48W• in 20 mM phosphate buffer, pH 7.2. Inset: Log−log plot showing microwave power saturation data for Az48W• (□) and ReAz108W• (●) with best-fit lines to eq 1.

Results

Absorption Spectra of Az48W• and ReAz108W•. The difference absorption spectrum of Az48W after photolysis with 280 nm light is presented in Figure 1 and compared to the difference absorption spectrum of ReAz108W• that was published previously. Both spectra were acquired after 180 s of photolysis. The Az48W• spectrum shows a bleach of the ground state tryptophan absorption at 290 nm and a bleach of the Cu(II) ligand-to-metal charge transfer (LMCT) band at 630 nm that is characteristic of oxidized blue copper proteins. This bleach is accompanied by an absorption increase in the spectral region reported for neutral tryptophan radicals, 486 and 516 nm.[11,44] Two isosbestic points at 430 and 527 nm persist throughout the duration of the photolysis (Figure 1, inset). These spectral features suggest that direct excitation of the tryptophan residue reduces the copper center and generates Az48W•, a neutral tryptophan radical. Az48W• persists for over 2 h, and the spectrum does not change under acidic or deuterated buffer conditions, as shown by the absorption and resonance Raman spectra (see Supporting Information, Figures S1 and S2). We discuss the stability of the radical and the origin of the main absorption bands further below.

Substitution of zinc for the copper center led to only a small absorbance from Az48W• (Figure 2, trace A). Photolysis experiments in the presence of N_2O, a solvated electron scavenger,[55] resulted in the bleach of the LMCT absorption band but no indication of Az48W• (Figure 2, trace B). Deoxygenation was necessary for generation of the long-lived Az48W• species, and control experiments using a tryptophan- and tyrosine-deficient azurin mutant indicated no change in absorbance spectra after photolysis (data not shown).

EPR Spectroscopy. The X-band first-derivative EPR difference spectra of both azurin radicals in frozen solution are presented in Figure 3. The zero crossing for both radicals occurs near a g-value of 2.0028, which is expected for an organic π-radical.[35] Minimal g-tensor anisotropy is observed; this result is typical for a radical with spin density only on light atoms such as carbon and nitrogen. Hyperfine structure is readily apparent in both EPR spectra. The Az48W• spectrum clearly shows additional hyperfine features at the wings of the spectrum and some anisotropy. By comparison, the spectrum of ReAz108W• is broadened and only shows a hint of bands at the wings. The spectrum of the Cu(II) ReAz108W• radical is identical to that previously published for the Zn-substituted ReAz108W• protein, suggesting that the line shape is not affected by the metal center.[44] Because saturation phenomena were observed at microwave powers of ~100 μW for Az48W•, low microwave powers of ~6 μW were employed to avoid broadening of the hyperfine features.

Simulations of the Az48W• and ReAz108W• spectra yield values for hfcc's (Figure 3 and Table 1) and reveal that the spin density is predominantly located on the nitrogen, C_3, C_5, and C_7 atoms, in agreement with prior reports.[35,38,39] The g-values of both radicals were constrained to those obtained at high field for ReAz108W• (g_{xx} = 2.00355, g_{yy} = 2.00271, g_{zz} = 2.00221);[44] this constraint resulted in satisfactory fits to the experimental data. The dominant hyperfine features are caused by coupling to the β-methylene protons (Hβ_1 and Hβ_2 at angles

(55) Head, D.; Walker, D. C. *Nature* **1965**, *207*, 517.

Table 1. EPR Simulation *g*-Tensor (g_{ii}) and Hyperfine Tensor (A_i in gauss) Principal Values for ReAz108W• and Az48W• from Fits of the EPR Powder Spectra (EPR parameters for tryptophan radical W111• in *E. coli* ribonucleotide reductase[35,38] are presented for comparison)

tryptophan radical	tensor element	g_{ii} [a]	A_i (^{14}N)	A_i (Hβ_1)	A_i (Hβ_2)	A_i (H5) [b]	A_i (H7) [b]	A_i (N...H−OH) [c]
ReAz108W•	*xx*	2.00355	≤1	2.1	11.5	−6.0	≤ |1|	−1.2
	yy	2.00271	≤1	1.5	14.3	−2.1	−7.9	1.9
	zz	2.00221	10.4	2.3	11.9	−4.8	−4.2	−0.8
	iso	2.00282	3.5−4.1	2.0	12.6	−4.3	−(4.0−4.4)	∼0
Az48W•	*xx*	2.00355	≤1	6.6	9.0	−7.1	−1.8	NA
	yy	2.00271	≤1	7.3	8.7	−1.8	−3.9	NA
	zz	2.00221	11.8	5.0	7.4	−2.9	−4.9	NA
	iso	2.00282	3.9−4.6	6.3	8.4	−3.9	−3.5	NA
RNR W111•[35,38]	*xx*	2.0031	<1	13.8	27	6.8	<1.0	−1.18
	yy	2.0031	<1	13.8	27.5	<1.0	6.1	1.93
	zz	2.0023	10.5	13.8	28.3	5	5.1	−0.79

[a] The *g*-tensor principal values were constrained to those values presented in Miller et al.[44] [b] Negative sign for ring proton values reflects positive carbon spin density;[59] the *x*-axes of H5 and H7 are rotated 30° with respect to *g*-tensor *x*-axis.[78] [c] Hyperfine tensor assigned to the proton of a hydrogen-bond donor to the deprotonated indole nitrogen. The hfcc's were constrained to values previously obtained for hydrogen-bonded tryptophan radicals.[35,38] A hydrogen bond was not applicable (NA) in the simulation of Az48W•.

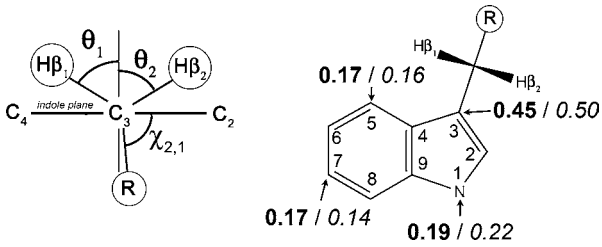

Figure 4. Left: Orientation of β-methylene protons Hβ_1 and Hβ_2 and the protein backbone R with respect to the tryptophan indole plane denoted by $C_2-C_3-C_4$. View is along the $C_\beta-C_3$ axis, where the C_β label is omitted from the figure for clarity. θ_1 and θ_2 are the dihedral angles of the β-methylene protons relative to the normal to the indole plane; $\chi_{2,1}$ is the dihedral angle of the tryptophan indole plane with respect to the protein backbone R ($\chi_{2,1} = \theta_2 + 30°$). *Right:* Molecular structure of the neutral tryptophan radical with numbering scheme and spin densities for ReAz108W• (bold) and Az48W• (italics). Spin densities on nitrogen reflect the average values within a plausible range (see main text for details).

θ_1 and θ_2, respectively, from the π-system; see Figure 4). Large anisotropic coupling to the indole nitrogen gives rise to the shoulders near the edges of the EPR spectrum, and this effect is most prominent in the case of Az48W•. The hfcc's found from the simulations are summarized in Table 1. A hydrogen bond with hfcc's constrained to values reported previously was included in the simulations of ReAz108W•, as discussed further below.[35]

Microwave power saturation experiments were performed to identify the power at half-saturation and to probe dipolar coupling between the tryptophan radical and copper in Az48W• and ReAz108W• (Figure 3, inset).[48] The EPR signal intensity was fit to eq 1,

$$S = K\frac{\sqrt{P}}{[1 + P/P_{1/2}]^{b/2}} \quad (1)$$

where S is the first-derivative peak-to-peak amplitude, K is a constant that depends upon parameters of the instrument, P is the microwave power, $P_{1/2}$ is the microwave power at half-saturation, and b is a parameter that depends on line broadening.[48] The best fit to the data yields a power at half-saturation ($P_{1/2}$) for Az48W• of 40 μW with $b = 1$; this value for b reflects an inhomogeneously broadened line in the absence of dipolar coupling to a paramagnetic ion.[48] The best fit to the ReAz108W• data gives a $P_{1/2}$ of 600 μW with $b = 1.1$.

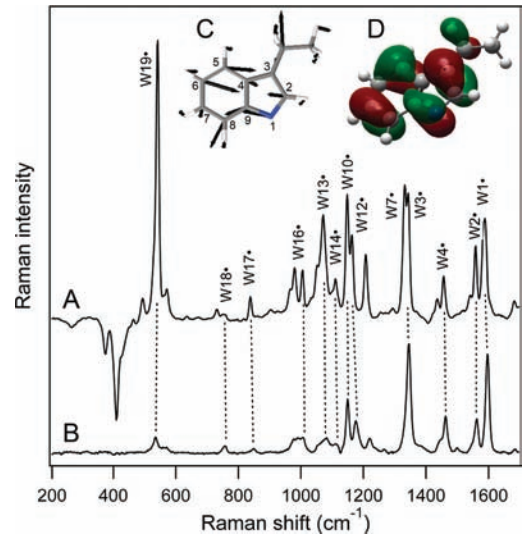

Figure 5. Resonance Raman difference spectra (514.5 nm excitation) of (A) Az48W• and (B) ReAz108W• in 20 mM phosphate buffer, pH 7.2. Spectra are offset for clarity and normalized to the W1• intensity. Insets: (C) Normal mode for W19• where displacement vectors are enlarged 5×. (D) Singly occupied molecular orbital (SOMO) of Trp•.

Resonance Raman Spectroscopy. The 514.5 nm resonance Raman difference spectra of Az48W• and ReAz108W• are shown in Figure 5. The positive peaks reflect vibrations of the radical. Negative peaks from the Cu(II)-ligand normal modes are also observed in the difference spectrum of Az48W•.[50] The resonance Raman frequencies and intensities differ for the two radical species. Most peaks are downshifted in Az48W• relative to ReAz108W• (Table 2). An intense peak at 542 cm^{-1}, which has been labeled W19• (see below), is observed in the spectrum of Az48W•; this mode intensity is weak in the 514.5 nm excitation RR spectrum of ReAz108W•. There are additional peaks in the RR spectrum of Az48W• that were not previously reported in the spectrum of ReAz108W•. These include a second band near the W3• mode, a band at 1111 cm^{-1}, and three resolved peaks near the strong W16• mode for both Az48W• and ReAz108W•. Additionally, the W17• mode is narrower and occurs at lower frequencies than previously reported.[19] The vibrational mode frequencies remain constant under different buffer conditions for both Az48W and Az48W• (Supporting Information, Figure S3). The comparison of calculations with

Table 2. Mode Assignments and Frequencies (cm^{-1}) of Tryptophan Radical Resonance Raman Bands for Az48W• and ReAz108W• (λ_{ex} = 514.5 nm) and the Frequency Differences between the Solvent-Exposed (ReAz108W•) and Buried (Az48W•) Tryptophan Radicals ($\Delta_{environment}$)[a]

mode	Az48W• pH 7(cm^{-1})	ReAz108W• pH 7 (cm^{-1})	$\Delta_{environment}$ (cm^{-1})
W1•	1588	1596	−8
W2•	1559	1563	−4
W5•	1492	1501	−9
W4•	1457	1463	−6
W3•	1342	1345	−3
W7•	1332	–	–
W12•	1163	1176	−13
W10•	1148	1149	−1
W14•	1111	1114	−3
W13•	1071	1082	−11
W16•	1006	1004	2
W17•	838	849	−11
W18•	752	756	−4
W19•	542	535	7

[a] The W7• mode was not identified in ReAz108W•.

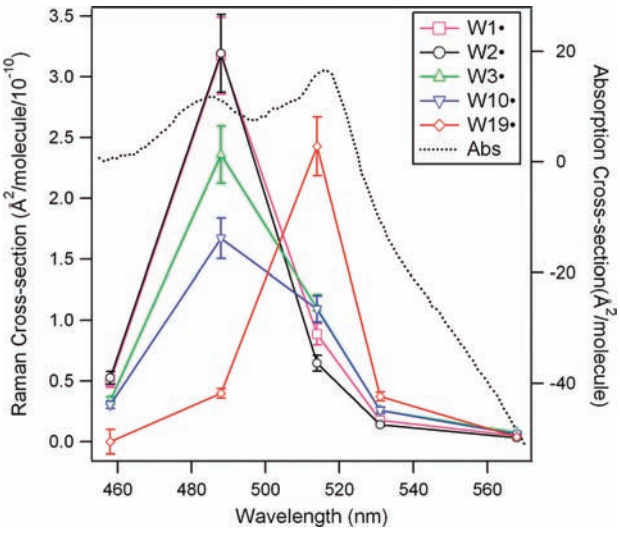

Figure 6. Resonance Raman cross sections for five vibrational modes and absorption cross section for Az48W• based on difference spectra. Negative absorption cross section reflects bleach of the copper signal.

experimentally observed values and depictions of these normal modes are presented in the Supporting Information (Figure S4 and Table S1). UVRR spectra of the closed-shell species Az48W were also acquired, and the results are presented in the Supporting Information (Tables S2 and S3).

The Raman excitation profiles are compared to the absorbance of Az48W• in Figure 6. The W1• and W2• cross sections are largest with 488 nm excitation. This excitation wavelength coincides with the high energy portion of the absorption band, and these cross sections are approximately 3-fold lower with 514.5 nm excitation. The cross sections of the W3• and W10• modes are also greatest with 488 nm excitation; however, the decrease with 514.5 nm excitation is less than 2-fold. In contrast, the cross section of the W19• mode is greatest with 514.5 nm excitation; this excitation wavelength overlaps with the second, low energy region of the absorption band.

Discussion

The present analysis of a tryptophan radical in a hydrophobic cavity with 0% solvent-exposed surface area (Az48W•) and one that is hydrogen-bonded to water in an ~40% solvent-exposed region of the protein (ReAz108W•) sheds new light on the effects of environment and conformation on magnetic, electronic, and vibrational spectral properties. The oxidized radical species is very sensitive to the protein environment and shows large systematic shifts for the absorption and resonance Raman bands. In contrast, the analogous closed-shell residues, tryptophan-48 and tryptophan-108, exhibit only subtle or nonsystematic spectral changes. The data for the radicals and subsequent analysis lay the foundations for a better understanding of the role of the protein matrix on radical reactivity. Furthermore, with knowledge of redox potentials and estimated electron transfer kinetics, we propose a rate and mechanism for the key deprotonation event that creates an unusually long-lived neutral tryptophan radical in a protein core.

Spin Densities and Conformations of Az48W• and ReAz108W•. EPR spectroscopy has been the prevailing technique for identification and determination of the structures of aromatic amino acid radicals in proteins.[7,8,38−42] The differences between the EPR spectra of ReAz108W• and Az48W• were analyzed with simulations to obtain hfcc's (Table 1), which in turn provided direct information on the spin densities and conformation of tryptophan radicals.[35] We emphasize at the outset that our simulations do not yield unique sets of anisotropic hfcc's for the two radicals, primarily because the experimental spectra are not well-resolved. A preferred set of parameters that yields a reasonable fit to the experimental spectra for Az48W• and ReAz108W• is shown in Table 1. We favor the set presented here not only because they result in simulated spectra that fit the experimental spectra well but also because the hyperfine coupling constants are consistent with prior literature on tryptophan radicals and aromatic systems in general. For example, we have constrained our anisotropic *g*-values for both Az48W• and ReAz108W• to those previously determined at high field for the latter radical species.[44]

The best-fit simulations for Az48W• and ReAz108W• were determined by constraining the β-protons to have nearly axial symmetry.[56] The hfcc's for the β-protons that we have selected are consistent with prior reports as well as theoretical studies on aromatic π-radicals.[39,57,58] The spin density on C_3 (ρ^{π}_{C3}) as well as the orientation of the tryptophan ring, defined by the dihedral angles θ for the two β-protons relative to the p_z orbital of the C_3 center (Figure 4), can be found using eq 2:[35,59]

$$A_{iso}(H_\beta) = \rho^{\pi}_{C3}(B' + B''\cos^2\theta) \qquad (2)$$

The values of $B' = 0$ G and $B'' = 58$ G are used in eq 2, as done by others, and the difference between the projection of the proton dihedral angles is constrained to 120°.[35] A spin density of $\rho^{\pi}_{C3} = 0.50$ is found for Az48W•, and dihedral angles θ_1 and θ_2 of −62° and 58°, respectively, are obtained for the two β-protons. This result implies a dihedral angle of the plane of the indole ring with respect to the protein backbone (R in Figure 4), $\chi_{2,1}$, of 88°; this geometry is consistent with the dihedral angle of 90° found in the crystal structure of wild-type azurin.[20] A spin density of $\rho^{\pi}_{C3} = 0.45$ is found for ReAz108W•. The dihedral angles obtained for the two β-protons are −74° and 46°, which gives a $\chi_{2,1}$ for ReAz108W• of 76°, comparable to the torsion angle of 82° that is found in the crystal

(56) Svistunenko, D. A.; Jones, G. A. *Phys. Chem. Chem. Phys.* **2009**, *11*, 6600–6613.
(57) McConnell, H. M.; Strathdee, J. *Mol. Phys.* **1959**, *2*, 129–138.
(58) McConnell, H. M.; Chesnut, D. B. *J. Chem. Phys.* **1958**, *28*, 107–117.

structure of ReAz108W.[44] The small 6° discrepancy may reflect differences between crystal packing and solution phase conformation as well as the error for the fit. The coupling constants to protons H_5 and H_7 on the indole ring and to the indole nitrogen are anisotropic as expected. Spin densities for Az48W• determined from these hfcc's are 0.16 for C_5 (ρ^{π}_{C5}) and 0.14 for C_7 (ρ^{π}_{C7}). The spin density at the nitrogen (ρ^{π}_{N}) ranges from 0.21 to 0.23. In this analysis, we use the following relationship between the dipolar coupling parameter $A'_{||}$ and spin density (eq 3):[35]

$$\rho^{\pi}_{N} = A'_{||}/95.6\ \text{MHz} = (A_{zz} - A_{iso})/(34.1\ \text{G}) \qquad (3)$$

The range of values for the spin density depends upon the magnitude of the isotropic coupling constant, which in turn depends upon $A_{xx} = A_{yy} = A_{perp}$. These axial components are too small to be determined from our spectra but are likely ≤ 1 G.[35] Similarly, spin densities for ReAz108W• are 0.17 for C_5, 0.17 for C_7, and 0.18−0.20 for N.

We also verified that the inclusion of a representative set of hydrogen-bond hfcc's also yielded a simulation for ReAz108W• that was an acceptable match to the experimental spectrum. We emphasize that our EPR spectra are not sufficiently resolved to give proof for a hydrogen bond to ReAz108W•; nonetheless, the inclusion of these hfcc's is reasonable in view of the evidence for a hydrogen bond from UV resonance Raman data, fluorescence data (see Supporting Information, Figure S2), and the crystal structures.[16,19,20,44] It is possible that this hydrogen bond to ReAz108W• may perturb the structure and electronic spin density of the neutral radical toward that of the cation radical.[19] In the limit of a protonated tryptophan radical, large decreases in ρ^{π}_{C3} and ρ^{π}_{N} and increases in ρ^{π}_{C5} and ρ^{π}_{C7} are predicted.[39] An ~15% change in the spin density at the nitrogen (0.22/0.19) in the expected direction is observed for the spin densities derived for ReAz108W• in comparison with Az48W•. However, these changes in spin density distribution do not account for the bulk of the observed differences in the EPR spectra. Instead, the orientation of the indole ring, which differs between the two azurin mutants, is the dominant influence on the shape of the EPR spectra.[35] Future experiments utilizing high-frequency and double resonance EPR techniques are expected to give a more accurate determination of the spin densities and *g*-values of these two tryptophan radicals.

Microwave power saturation experiments were employed to characterize exchange and dipolar coupling between unpaired spins.[48] These experiments have generally been replaced by pulsed EPR experiments that measure saturation recovery; however, the CW-EPR power saturation experiment is readily available in our lab and has been shown by others to yield quantitative insights on the spin−spin interaction between neighboring metal centers or metal-radical systems.[3,48,60] The best-fit curve for the dependence of the peak-to-peak signal amplitude of Az48W• on power yielded a $P_{1/2}$ of 40 μW, which is at least an order of magnitude lower than that observed previously for a tryptophan radical located 10 Å from a paramagnetic iron center in a peroxidase protein.[3] The low value of $P_{1/2}$ measured here indicates a lack of spin−spin interactions in Az48W• and therefore suggests an intraprotein ET reaction generates a tryptophan radical and diamagnetic Cu(I) center. Microwave saturation experiments on ReAz108W• indicate a much higher saturation power of 600 μW; this value is similar to that observed for tryptophan radicals in the presence of heme cofactors.[3] The increased power required for EPR saturation of this radical is likely due to spin−spin relaxation facilitated by the paramagnetic Cu(II) center that is located 20 Å away from the tryptophan radical at position 108.[44]

Absorption Differences between ReAz108W• and Az48W•. The Az48W• absorption spectrum undergoes an ~23 nm hypsochromic shift relative to ReAz108W• and other neutral tryptophan radicals in aqueous solution and in proteins.[2,11,44] The absorption bands of Az48W• are also blue-shifted by ~60 nm relative to those expected for a cation radical.[11] The electronic absorption data clearly show that Az48W• is a non-hydrogen-bonded neutral tryptophan radical, consistent with its location in a hydrophobic cavity within azurin. The absorption shifts observed for the radical are significantly greater than those observed for the closed-shell tryptophan residues in Az108W and Az48W (see Supporting Information, Figure S2) or tyrosine radical absorption maxima in different solvent environments.[61] Evidently, the tryptophan radical absorption frequency is an unusually sensitive reporter of local environment, hydrophobicity, and/or hydrogen-bonding. Another novel finding from our work is the presence of two peaks in the absorption spectrum of the radical with distinct Raman excitation profiles. These features can be attributed to distinct electronic transitions or a vibrational progression. Our interpretation of the absorption spectrum in the context of the resonance Raman excitation profile is discussed below.

We assume that each tryptophan radical that persists on the time scale of the experiment causes reduction of Cu(II) to Cu(I). Spin integration of the EPR spectra also supports near-quantitative reduction of Cu(I) for each Az48W• radical generated. By invoking the known extinction coefficient of Cu(II) azurin (5900 M^{-1} cm^{-1}), a lower limit on the extinction coefficients for the two peaks of Az48W• can be calculated: ε(486 nm) ≈ 950 M^{-1} cm^{-1} and ε(516 nm) ≈ 1250 M^{-1} cm^{-1}.[62] These values are approximately 2-fold lower than the extinction coefficients of 1750−2300 M^{-1} cm^{-1} that were previously determined for neutral tryptophan radicals in aqueous solution using pulse radiolysis.[11] Our new values are likely more accurate than those reported previously because of the inclusion of the copper(II) absorbance as an internal standard. However, it is also possible that the variation in extinction coefficient is influenced by the nonpolar protein environment, relative to the aqueous environment of the prior work. Our estimates also do not take into account any decay of Az48W• that occurs between photolysis and measurement of the absorption spectrum; however, this effect is expected to be minimal based on the time scale of the measurement (approximately 5 min) relative to the lifetime of the radical (over 2 h).

Changes in Resonance Raman Frequencies and Intensities between Az48W• and ReAz108W•. Resonance Raman frequencies are sensitive to small changes in solvent interaction, hydrogen bonding, and π-electron density.[18,51,63] The RR spectra of Az48W• and ReAz108W• clearly show that the protein environment exerts a strong influence on the vibrational frequencies and band intensities of tryptophan radicals. In fact,

(59) McConnell, H. M. *J. Chem. Phys.* **1956**, *24*, 764–766.
(60) Eaton, G. R.; Eaton, S. S. In *Distance Measurements in Biological Systems by EPR*; Berliner, L. J., Eaton, G. R., Eaton, S. S., Eds.; Kluwer Academic Plenum Publishers: New York, NY, 2000; Vol. 19, pp 29−154.
(61) Joshi, R.; Mukherjee, T. *Biophys. Chem.* **2003**, *103*, 89.
(62) Goldberg, M.; Pecht, I. *Biochemistry* **1976**, *15*, 4197–4208.
(63) Hu, X.; Spiro, T. G. *Biochemistry* **1997**, *36*, 15701–15712.

the frequency decreases observed in the visible RR spectrum of Az48W• relative to ReAz108W• are greater than the corresponding shifts of the closed-shell species as determined by UVRR spectroscopy (see Supporting Information, Table S2). These general downshifts suggest perturbation of the π-electron density around the indole ring. The systematic variation in vibrational frequencies as well as the significant blue shift in the absorption spectra for the Az48W• radical may, in part, be due to lack of an indole hydrogen bond. Alternatively, the presence of $\pi-\pi$ interactions between Az48W• and a phenylalanine residue at position 110 could also perturb the electron density. Variations in relative Raman cross sections of bands reflect different resonance enhancement factors at the excitation wavelength; 514.5 nm coincides with the low energy absorption peak for Az48W•, whereas the same wavelength lies near the higher energy absorption band for ReAz108W•.

The RR spectrum of Az48W• in comparison to the ReAz108W• allows the identification of modes that are most sensitive to solvent and/or protein environment and hydrogen bonding. These include the bands assigned as W1•, W5•, W12•, W13•, and W17•. Each of these modes decreases in frequency 8 to 13 cm^{-1} for the non-hydrogen-bonded radical in a nonpolar environment. The former four modes predominantly involve ring breathing and stretching displacements, suggesting that the π-bonding electron density on Az48W• is altered from that of ReAz108W•. The presence of strong $\pi-\pi$ interactions between Az48W• and nearby residues may contribute to these observed shifts. The W17• mode, which involves significant nitrogen displacement, serves as a hydrogen-bonding indicator.[18,19] The frequency of this mode is observed to increase with N−H bond strength, which reflects increased hydrogen bonding to the tryptophan radical.[19] The -11 cm^{-1} shift observed for Az48W• compared to ReAz108W• is consistent with the absence of a hydrogen bond to the indole nitrogen of Az48W• and agrees with prior observations.[19]

The W3• mode, which consists of predominantly C_2-C_3 stretching character, is one of the most prominent signatures of the radical and is also a good indicator of its protonation state.[19] The 212 cm^{-1} downshift in W3• frequency relative to closed-shell tryptophan supports the assignment of Az48W• to a neutral species. An additional band near the W3• mode is observed and has been assigned to the W7• mode, which is a benzene-like stretching mode that was previously unidentified in the ReAz108W• radical due to overlap with the intense W3• band. This assignment agrees with our calculations and a prior study that reports the W7• mode near 1330 cm^{-1}.[43] The Az48W• spectrum also allows the assignment of the W14• mode, which consists primarily of $N-C_2$ stretching character. The closed-shell W14 mode is predicted to shift $+40$ cm^{-1} upon oxidation, and the assignment of the radical peak at 1111 cm^{-1} to W14• agrees with the predicted value and expected frequency increase for this mode. Additionally, this mode shows significant nitrogen displacement, suggesting that this peak should shift in different hydrogen bonding or solvation conditions. The observation that the 1114 cm^{-1} band in the RR spectrum of solvent-exposed ReAz108W• is influenced by acidic pH or deuterated buffer, as reported in a previous publication, supports the assignment of this band.[19] Improved experimental conditions have allowed the resolution of three peaks near the strong W16• mode for both Az48W• and ReAz108W•; in contrast to our prior report, the current spectra have no residual phosphate buffer peaks. The W17• mode is also affected by this procedure. This mode is now observed to be narrow and downshifted considerably for the radical species relative to the closed-shell tryptophan, which is in better agreement with calculations.

The predominant spectral change between the RR spectra for Az48W• and ReAz108W• with 514.5 nm excitation is the appearance of a high intensity peak at 542 cm^{-1} for Az48W•. In the UVRR spectrum of closed-shell tryptophan, a small peak is also observed in this spectral region; however, the 542 cm^{-1} mode has not been assigned according to the standard tryptophan mode nomenclature. We have labeled this mode W19 and W19• for the closed-shell and radical species, respectively. The mode is best described as an in-plane benzene/pyrrole ring breathing distortion, but it also involves significant displacement of the C_β nucleus in the protein backbone (Figure 5, inset C). This mode is expected to downshift upon formation of the radical, as observed experimentally. As a starting point to explain the strong enhancement of the W19• mode, we examine the singly occupied molecular orbital (SOMO) of the tryptophan neutral radical (Figure 5, inset D). This orbital shows extended electron density onto the backbone atoms;[64] thus, one can reasonably expect enhancement of a mode that includes significant C_β displacement. We are pursuing additional calculations to obtain electron density difference maps for the relevant electronic transitions of the tryptophan neutral radical.

RR intensities reflect structure and dynamics and report on vibrational modes that are Franck−Condon coupled to the electronic excitation(s).[50,65] Modes that have significant displacement in the resonant excited state are enhanced in RR spectroscopy. For Az48W•, the absorption band shows two distinct peaks at 486 and 516 nm (Figure 1), and the RR intensities for the most intense vibrational modes exhibit differential enhancement across these absorption peaks (Figure 6). The Raman excitation profiles indicate that the high-frequency W1• and W2• intensities overlap with the high energy portion of the absorption band, W3• and W10• intensities overlap with both bands, and the low-frequency W19• profile coincides with the low energy region of the absorption. Dispersion in the peak positions of Raman excitation profiles can have a number of origins. For example, Raman excitation profiles for some modes of closed-shell tryptophan reveal differential vibronic coupling to nearby electronic excited states.[66] While existing theoretical treatments do not show evidence of multiple transitions in the visible absorption of the radical,[64,67] we consider it plausible that two or more electronic transitions give rise to the variation in the excitation profiles. The features in the visible absorption spectrum may also arise from a vibrational progression. This interpretation is also feasible based on the observation that the two peaks are relatively narrow and spaced $\sim$1200 cm^{-1}, close to the frequency of the several strong resonantly enhanced radical modes. In this case, relatively large Franck−Condon factors for low frequency modes may give rise to the observed dispersion. Additional measurements and calculations are ongoing to unambiguously discern these and other possible origins for the Raman excitation profiles observed here for Az48W•.

(64) Crespo, A.; Turjanski, A. G.; Estrin, D. A. *Chem. Phys. Lett.* **2002**, *365*, 15–21.
(65) Myers, A. B.; Mathies, R. A. In *Biological Applications of Raman Spectroscopy, Vol. 2: Resonance Raman Spectra of Polyenes and Aromatics*; Spiro, T. G., Ed.; John Wiley and Sons: New York, 1987; Vol. 2.
(66) Asher, S. A.; Ludwig, M.; Johnson, C. R. *J. Am. Chem. Soc.* **1986**, *108*, 3186–3197.
(67) Evleth, E. M.; Chalvet, O.; Bamiere, P. *J. Phys. Chem.* **1977**, *81*, 1913–1917.

Proposed Electron Transfer Mechanism and Proton Transfer Pathways. We now address the question of the mechanism of tryptophan radical generation. At long times, it is clear from our steady-state absorption experiments that the formation of the tryptophan radical is associated with reduction of the nearby Cu(II) center. Furthermore, the EPR power saturation experiments reveal that the electron transfer must have occurred *intramolecularly*, since an *intermolecular* process cannot explain the low power saturation for Az48W•. The intramolecular reduction may occur by one of two mechanisms: (1) direct electron transfer from the photoexcited tryptophan residue or (2) indirectly by a solvated electron that is photoejected from tryptophan. We argue against the second possibility because the presence of saturated N_2O did not affect the reduction of Cu(II). Thus, the aqueous solvated electron is unlikely to be the reducing agent, which is consistent with the solvent-excluded location of the W48 residue. Instead, association between N_2O and the protein matrix appears to quench the long-lived tryptophan radical, though the details of this interaction have not been determined. Substitution of redox-inactive zinc, which eliminates a direct ET pathway altogether, reduced the efficiency of tryptophan oxidation by 80%. Therefore, in the copper(II) protein, we estimate that a solvated electron route contributes much less than 20% to the overall mechanism of copper(II) reduction, and the dominant path in Az48W is one that involves direct ET. Previous reports on the fluorescence quenching of tryptophan-48 in holoazurin have invoked either energy transfer or electron transfer to the metal center.[24,25] In other protein systems, even those without nearby exogenous electron or energy acceptors, tryptophan fluorescence is known to be quenched by electron transfer to the amide backbone.[68] Therefore, a proposal of direct electron transfer from tryptophan-48 to Cu(II) through the amide backbone is consistent with previous studies.

The accumulation of Az48W• and Cu(I) as a function of photolysis time allows modeling of the kinetics associated with the ET reaction. We estimate an electron transfer rate between excited-state tryptophan-48 and copper(II) to be $\sim 10^9$ s^{-1} (see Supporting Information).[24,69,70] Other groups have studied possible electron transfer pathways through azurin to the copper center using the disulfide bond or a gold electrode as the electron donor.[21,71] Experiments based on photolysis of the disulfide bond imply an ET route through Trp-48 and Val-49 to Cys-112 and Cu(II) via a hydrogen bond,[21] while ET in azurin adsorbed on a gold electrode relies on the backbone conformation of Trp-48.[71] In our experiments, the electron from the indole π-system of Trp-48 may tunnel through the backbone to the copper center by either or both of these proposed pathways (Figure 7): (1) an 8-bond pathway from indole to copper that requires tunneling through a 3.61 Å hydrogen bond between Asn-47 and Cys-112 (consistent with the electrode work) or (2) an 11-bond pathway to Cu(II) *via* Val-49 that requires tunneling through a hydrogen bond of 2.82 Å (consistent with the disulfide work). In either case, the nonbonded distance from Trp-48 to Cu(II) is short (10 Å), and the electron transfer rate is expected to be high.[70,72]

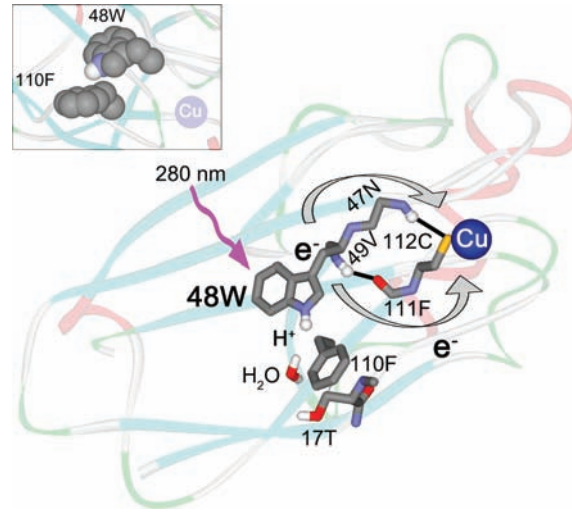

Figure 7. Crystal structure of azurin (4AZU) showing residues involved in proposed proton and electron transfer pathways. Inset: Space-filling model of $\pi-\pi$ interactions between Trp-48 and Phe-110 in protein interior.

A high forward electron transfer rate is not sufficient for the formation of the long-lived tryptophan neutral radical and reduced copper center. In fact, the back electron transfer from the reduced copper center to the tryptophan cation radical Az48W$^+$• is predicted to be faster than the forward electron transfer due to the high driving force and low reorganization energy.[70] Therefore, we expect that most of the Cu(I)-Az48W$^+$• initially generated will rapidly decay back to Cu(II)-Az48W. Analysis of radical concentration as a function of photolysis conditions and time provides an estimate of the quantum yield of 10^{-4} for radical production. To stabilize the long-lived tryptophan radical that is observed, deprotonation of the cation radical, which has a p$K_a \approx 4$,[11] is necessary. Based on the estimated forward and back electron transfer rates from semiclassical ET theory,[69] the deprotonation rate, k_{deprot}, is predicted to be 5×10^6 s^{-1} (see Supporting Information). This rate is a calculated extrapolation from the steady-state accumulation of Az48W• and is similar to that observed for the deprotonation of tryptophan radicals in aqueous solution[73] or in DNA photolyase.[2]

An important question remains: how does the tryptophan radical lose a proton after it has transferred an electron to Cu(II)? A direct loss of a proton to the solvent is highly unlikely, because the tryptophan residue is encapsulated in a solvent-excluded cavity of the protein. Instead, the following proton transfer pathway is proposed. In the ground state, the indole proton is positioned to participate in a cation-π-like interaction with a phenylalanine residue at position 110 (110F) (Figure 7, inset); UV resonance Raman frequencies and intensities of Az48W support $\pi-\pi$ interactions between 48W and 110F.[74,75] Following photoinduced ET, this proton may transfer to 110F. Threonine-17 (17T), which is only ~5 Å from 110F, can also

(68) Callis, P. R.; Liu, T. Q. *J. Phys. Chem. B* **2004**, *108*, 4248–4259.
(69) $E(Trp^{\bullet+}/Trp) = 1.15$ V, $E(Cu^{II/I}) = 0.31$ V, $E(Trp^*) = 4.03$ eV, $E(Trp^{\bullet+*}) = 2.19$ eV, $\lambda(Cu^{II/I}) = 0.7$ eV, and $\lambda(Trp^{\bullet+}/Trp) = 0.1$ eV.[24,70]
(70) Page, C. C.; Moser, C. C.; Chen, X.; Dutton, P. L. *Nature* **1999**, *402*, 47.
(71) Yokoyama, K.; Leigh, B. S.; Sheng, Y. L.; Niki, K.; Nakamura, N.; Ohno, H.; Winkler, J. R.; Gray, H. B.; Richards, J. H. *Inorg. Chim. Acta* **2008**, *361*, 1095–1099.
(72) Gray, H. B.; Winkler, J. R. *Annu. Rev. Biochem.* **1996**, *65*, 537–561.
(73) Bent, D. V.; Hayon, E. *J. Am. Chem. Soc.* **1975**, *97*, 2612–2619.
(74) Okada, A.; Miura, T.; Takeuchi, H. *Biochemistry* **2001**, *40*, 6053–6060.
(75) Xue, Y.; Davis, A. V.; Balakrishnan, G.; Stasser, J. P.; Staehlin, B. M.; Focia, P.; Spiro, T. G.; Penner-Hahn, J. E.; O'Halloran, T. V. *Nat. Chem. Biol.* **2008**, *4*, 107–109.

act as a proton acceptor,[76] and this solvent-exposed residue may promote release of the proton to solvent. We propose that the hydrophobicity of the tryptophan local environment destabilizes the intermediate tryptophan cation radical, and release of the proton is energetically favorable. Back electron transfer from Cu(I) to neutral Az48W• to generate the $Az48W^-$ anion product is unfavorable, particularly within the hydrophobic protein environment. The inability to form the anion product is supported by the observation that the closed-shell pK_a of tryptophan is ~17.[77] Therefore, we propose that the Az48W• neutral radical is kinetically stable after deprotonation.

Summary

Aromatic amino acid radicals are integral to a variety of biological ET reactions. Understanding the role of the protein matrix on the reactivity of these intermediates is a critical, and very challenging, area of research. Here, we have employed electronic, vibrational, and magnetic resonance techniques coupled with calculations to characterize neutral tryptophan radicals in two well-defined protein environments: a hydrophobic core and a solvent-exposed region. This comprehensive multi-spectroscopic approach enables the identification of features that are most sensitive to local environment and conformation. EPR and vibrational data support the presence of a hydrogen bond for the solvent-exposed radical and provide structural details of conformation and bond order. The absorption spectra are similarly sensitive to local environment and show an unusually large blue shift of over 20 nm for the nonpolar region of the protein. The absorption spectrum has distinct features, and Raman excitation profiles coincide with different regions of the absorption band. Finally, the generation of a neutral radical in a hydrophobic core is possible because of fast, intramolecular electron transfer to the copper center combined with a deprotonation event that occurs on the time scale of 200 ns; our observation that this radical is long-lived suggests a large barrier for reprotonation. These results provide fundamental insight into the spectral properties of tryptophan radicals and will help enhance our understanding of the reactivity of these important ET intermediates.

Acknowledgment. The authors would like to thank Tran Ha and Nicholas Don-Doncow for assistance with sample preparation, Roger Isaacson for advice on EPR calibrations, and Harry Gray for insightful discussions and feedback on the manuscript. H.S.S. was supported by an NDSEG graduate fellowship. This work was supported by the National Science Foundation CHE-0911766 to J.E.K.

Supporting Information Available: Supplemental materials and methods, description of electron transfer and deprotonation model, absorption and resonance Raman spectra of Az48W• and Az48W under different buffer conditions, fluorescence spectra of closed-shell azurin mutants, depictions of calculated normal modes for closed-shell and neutral radical of 3-ethylindole, and tabulated resonance Raman frequencies. This material is available free of charge via the Internet at http://pubs.acs.org.

JA101322G

(76) Ippolito, J. A.; Alexander, R. S.; Christianson, D. W. *J. Mol. Biol.* **1990**, *215*, 457.
(77) Balón, M.; Carmona, M. C.; Muñoz, M. A.; Hidalgo, J. *Tetrahedron* **1989**, *45*, 7501.
(78) Pogni, R.; Baratto, M. C.; Teutloff, C.; Giansanti, S.; Ruiz-Duenas, F. J.; Choinowski, T.; Piontek, K.; Martinez, A. T.; Lendzian, F.; Basosi, R. *J. Biol. Chem.* **2006**, *281*, 9517–9526.